(This article is a preprint of the final article that appeared in the 1995 IEEE Ultrasonics Symposium Proceedings, pp. 1617-1622)

NONLINEAR MODELING OF THERAPEUTIC ULTRASOUND

G. Wojcik, J. Mould, Jr., F. Lizzi*, N. Abboud, M. Ostromogilsky*, and D. Vaughan

Weidlinger Associates
4410 El Camino Real, Suite 110, Los Altos, CA 94022
333 Seventh Ave., New York, NY 10001

*Riverside Research Institute
330 West 42nd St. New York, NY 10036

ABSTRACT

We describe experimental finite element modeling of tissue ablation by focused ultrasound. Emphasis is on nonlinear coupling of high intensity sound, temperature, and tissue properties. The numerical basis for modeling nonlinearity is an incrementally linear, time-domain, finite element algorithm solving the electromechanical and bioheat equations in 2D/3D inhomogeneous elastic and acoustic media. Nonstandard modeling issues examined include harmonic generation/absorption and focal "bubble" evolution with consistent sound and thermal redistribution. The nonlinear pressure-density relation generates harmonics that increase absorption and heating, particularly in the focal zone. In the tissues modeled, harmonic heating is negligible for peak focal intensities of a few kW/cm^2. As the focal hot spot ablates tissue it may also generate "bubbles." Prefocal growth of a bubbly region is modeled using a simple boiling threshold and strong coupling between the scattered ultrasound and temperature redistribution as the region spreads. Generally, these experiments are intended to develop a more comprehensive modeling basis for quantifying tissue ablation phenomenology.

INTRODUCTION

The ability of ultrasound to safely penetrate deep into soft tissue has prompted its use for noninvasive therapies like hyperthermia and extracorporeal shock wave lithotripsy. This ability also makes noninvasive surgical applications feasible, using focused ultrasound to deliver intense vibrational energy to a small region of tissue with no significant effect on intervening and surrounding tissues. Friction raises tissue temperature in the focal region to relatively high values, causing confined coagulative necrosis and/or "cavitation." This process of thermal ablation provides a functional, noninvasive surgical technique by virtue of destroying tissue in a well defined target zone distant from the transducer.

Thermal ablation was first demonstrated in the early 1950s [1] and has since been applied to deep brain tumors [2], liver cancer [3], ocular therapy [4,5], and benign prostatic hypertrophy (BPH) [6], among others—but on a relatively limited basis. More widespread use requires advances in technology and hardware so the modality is demonstrably safe, reliable, and effective across a range of therapies. However, despite nearly 45 years of continuous study, significant uncertainties remain. For example, Fry [7] describes two modes of behavior depending on intensity. Either 1) the lesion expands uniformly by continuous thermal coagulation or 2) gas generation abruptly changes conditions and rapidly extends the pre-focus lesion towards the source. Lizzi et. al [8] explain the latter as effects of a gas body at the focus produced by vaporization, thermal degassing, or cavitation. They contend that this is the limiting factor in lesion control for very high intensity beams and conclude that gas body formation warrants further investigation [9]. Although Fry and Lizzi present cavitation as anomalous, Vallancien, et. al [10] tout it as the operative mechanism for coagulative necrosis in their apparatus. Our current level of understanding therefore invites conflicting interpretations, hence, uncertainties in treatment protocols that effectively limit the technique.

To further develop and qualify tissue ablation by focused ultrasound it is essential that we obtain a better understanding of the tissue response phenomena. They are fundamentally nonlinear since the initial focused beam rapidly changes tissue absorption and wave speed, which change beam focus and promotes scattering, which change tissue properties, and so on. This complexity has precluded comprehensive model studies of thermal ablation. Linear models are used [5,11] effectively, but cannot reproduce treatment-limiting behavior, while nonlinear models [12], e.g., based on the KZK equation [13], are currently too idealized for application to scattering, cavitating focal tissue.

The solution we propose is a discrete numerical model that is not limited by common mathematical and material idealizations. Furthermore, it must be versatile and easily applied by researchers and manufacturers who need to design safer, faster therapy protocols and transducers. Our basis is PZFlex [14], a 2D/3D, time-domain finite element code for electromechanical analysis that is widely used by the U.S. ultrasound system industry for linear, transient transducer modeling. PZFlex was originally developed for large-scale propagation, structural dynamics, and nonlinear modeling, hence, provides a near-ideal foundation for the present work.

This paper examines a number of modeling issues, including focused transducer design, the relevance of shocking in water and tissue, increased focal heating from nonlinearity, and evolution of "bubbly" regions emanating from the focal zone. Our work is in preparation for quantitative validations against laboratory experiments. It is expected that the following model results and general analysis techniques will help us understand anomalous focused ultrasound phenomena, highlight critical tissue characterization needs, augment experiment planning and interpretation, and help optimize treatments. Last but not least, it may reduce the number of in vivo experiments and sacrificed animals currently necessary to validate different focused ultrasound treatments.

FOCUSED TRANSDUCER

The canonical focused ultrasound transducer is an unbacked spherical cap mounted in a fixture. The element may be solid piezoceramic, annular, or composite. Flat phased arrays are also used for their dynamic focus and scan capability. In the simple case of axial symmetry, the transducer and complete propagation path can often be modeled with a discrete method, depending on f-number and frequency. It is otherwise necessary to divide the model into coupled zones, e.g., the *transduction* zone, the linear *propagation* zone, and the nonlinear *focal* zone. For example, from

a given transduction zone model we save the local radiated field, i.e., just above the element, extrapolate this through the medium (analytically or numerically) to near the focal zone, and apply the extrapolated field as input to the focal zone model.

A global modeling example is shown in Figure 1 for a low frequency, deep penetration transducer with 10 cm aperture and focal length (f/1), suggested by [15]. The radially poled spherical cap is 2 mm thick PZT-5H with its fundamental thickness resonance at 1 MHz. The cap is fixed to an aluminum baffle plate along the outer edge and the surfaces are water-loaded on the front and air-loaded on the back. Ten equal-area electrodes define annuli on the front face while the back electrode is continuous. For this example the transducer is driven at its 1 MHz resonance either uniformly or with a 72° phase delay between electrodes to extend the focus.

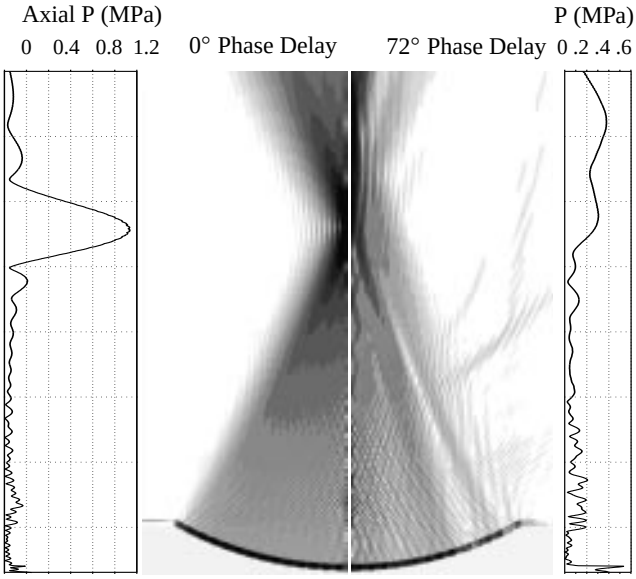

Figure 1. Calculated field and on-axis pressure from a radially poled, 2 mm thick, PZT-5H spherical cap with 10 cm aperture and radius (f/1). Ten equal-area annular electrodes are driven by 1.0 volt at 1.0 MHz, uniformly (left) or phased array (right).

Amplitude distributions for the two driving cases are shown on the left (uniform) and right (phase delayed) of Fig. 1, including on-axis pressure plots. Diffractions produced by the phase delay and localized vibrational modes in the transducer produce a fairly complicated pressure pattern on the right. The distinct beams and side lobes, particularly from the thin annuli near the edge, effectively disappear when the transducer is driven uniformly as shown on the left. This example is part of a study of cross-talk mechanisms in variable focus arrays. We note that isolation of annuli by air-filled kerfs turns out to be a poor solution because of coupled lateral modes in the rings. Although this is a relatively low frequency example, the model is similar to higher frequency designs, e.g., to a 4 MHz transducer with 2.5 cm aperture and focal length [5].

NONLINEAR MODELING

Nonlinearities arise in focused ultrasound because a tissue's mechanical and thermal properties depend on pressure, temperature, stress, strain, strain rate, etc. In order to model these nonlinear dependencies in a general, "production" setting, engineers have found incrementally linear numerical solutions of the governing partial differential equations (PDEs) especially useful. This approach is in contrast to formulating and solving PDEs that exhibit the nonlinearities explicitly. An example of the latter is the KZK equation for 2D shock propagation, which is a parabolic approximation of a hyperbolic PDE, hence, limited to one-way, paraxial propagation. Although very effective for numerical studies of shocks in uniform acoustic media, this approach does not readily generalize to propagation *and* scattering in inhomogeneous acoustic *and* elastic media. Incrementally linear forms of the elasticity equations have proven much more practical for "routine" engineering analyses.

For time-dependent phenomena, incrementally linear means the process of advancing a solution in time by discrete increments and modifying material properties at the end of each according to the instantaneous and/or historical (integrated) state of the material. Time increments are chosen so small that the solution is linear to first order over each increment. Although this approach is awkward analytically, it is ideally suited to numerical solution, particularly of transient phenomena.

Consider nonlinear propagation. Wave phenomena are naturally integrated in time using a time step Δt smaller than the CFL limit. For finite elements this is the shortest wave transit time between neighboring element corners (nodes) in the grid. The small step insures that wave nonlinearities are well-modeled by the incrementally linear approach, even very intense waves from explosions [16]. Wave speed c is inherently pressure-dependent by virtue of the nonlinear pressure p and density ρ relationship, namely

$$c \equiv \sqrt{\left.\frac{\partial p}{\partial \rho}\right|_s} \quad , \quad p = p_0 + A\left[\vartheta + \frac{B}{A}\frac{\vartheta^2}{2}\right] \quad , \quad \vartheta \equiv \frac{\rho}{\rho_0} - 1 \qquad (1)$$

where ϑ is dilatation, i.e., expansion, $A \equiv \rho_0 c_0^2$, B/A is the "parameter of nonlinearity" in the truncated Taylor series [17], and subscripts 0 and S refer to the ambient condition and a reversible (constant entropy) process, respectively. The incrementally linear, 2nd order accurate, explicit algorithm used here for nonlinear propagation is based on velocity and force update equations for a computational element written as

$$v^n = v^{n-1} + \frac{\Delta t F^{n-\frac{1}{2}}}{m} \Rightarrow u^{n+\frac{1}{2}} = u^{n-\frac{1}{2}} + v^n \Delta t \Rightarrow \vartheta^{n+\frac{1}{2}} = div\, u^{n+\frac{1}{2}} \qquad (2)$$

$$p^{n+\frac{1}{2}} = p_0 + A\left[\vartheta^{n+\frac{1}{2}} + \frac{B}{A}\frac{(\vartheta^{n+\frac{1}{2}})^2}{2}\right] \quad \Rightarrow \quad F^{n+\frac{1}{2}} \qquad (3)$$

where v^n, $u^{n\pm1/2}$, and $F^{n\pm1/2}$ are nodal velocity, displacement, and force, respectively, m is lumped mass, Δt is time step, and superscripts refer to time level, e.g., at $(n+1/2)\Delta t$. Note that pressure is an element-centered quantity and its integration over the element cross-section and uniform lumping yields the nodal force update implied in (3). This is an explicit formulation, hence, conditionally stable, i.e., the time step must be smaller than the CFL limit.

Equations (2) and (3) constitute a small-deformation algorithm, whence dilatation is calculated to first order as the divergence of displacement. This is appropriate when Mach number M, the ratio of particle velocity v to wave speed c, is small, i.e., $M \equiv v/c \approx P/(\rho c^2) << 1$, so that signal speed v+c is approximately equal to c. Small-deformations limit the code to relatively weak shocks, e.g., in contrast to high-explosive shocks. Nonetheless, it is adequate for virtually all therapeutic applications. For example, Mach number in water for a 6.8 MPa (1000 psi) plane wave is M ≈

0.004. A large-deformation generalization readily accommodates any exceptional cases [16].

For transient thermal modeling we solve the incrementally linear form of the bioheat transfer equation, i.e., Pennes equation [18]. This PDE is parabolic and integrated in time using implicit (unconditionally stable) algorithms for reasons of practicality. For accuracy, time step Δt is chosen to resolve the problem's highest temporal gradients. These depend on initial conditions and thermal parameters, or the time scale of nonlinearities. The discrete form of Pennes equation in the electro-mechanical-thermal version of PZFlex is

$$\left(\frac{2}{\Delta t}\boldsymbol{M}+\boldsymbol{K}\right)T^{n+1}=F^{n+1}+\boldsymbol{M}\left(\frac{2}{\Delta t}T^{n}+\tau^{n}\right) \qquad (4)$$

$$\tau^{n}\equiv\frac{2}{\Delta t}(T^{n}-T^{n-1})+\tau^{n-1} \qquad (5)$$

where T^n is the nodal temperature vector, τ^n is the rate of change vector, **M** and **K** are the capacity and conductivity matrices, respectively, F is the heat load vector, and superscripts refer to time level. Perfusion contributes to both **K** and F. Temperature-dependent thermal and/or perfusion properties are accommodated by incrementally changing the constitutive parameters in **M**, **K,** and F.

ATTENUATION ISSUES

Soft tissue attenuates ultrasound by intrinsic absorption as well as scattering from small-scale structure. Absorbed ultrasound expressed as heat is, of course, the basis for focused ultrasound therapy. Attenuation mechanisms in tissue are legion and our understanding remains incomplete. Nonetheless, for ultra-sound in the megahertz range the totality of mechanisms is reasonably approximated over a useful range of frequency f by the tissue-specific power law, $\alpha = \alpha_a + \alpha_s = af^b$, where a and b are constants. For example, in water the exponent is b=2 above 3 MHz, in muscle it is close to b=1+, and in fatty tissue it is around b=1.5. Although attenuation coefficient α includes bulk scattering, this is not explicitly included in our model. Hence, secondary absorption of incoherent, scattered energy is ignored. Note that various scales of statistical variation in element mass and stiffness can produce useful scattering.

The three media considered in our calculations are water and two tissues—muscle/tumor (T1) and fatty (T2). Power law constants are listed in Table 1, as well as nonlinearity parameters. A comprehensive source of tissue data is Duck [19].

Medium	a (dB/cm/MHz^b)	b	B/A
Water	0.0022	2.0	5.0
T1: Muscle/tumor	0.7	1.1	7.5
T2: Fatty tissue	0.75	1.5	10.0

Table 1. Attenuation, and nonlinearity parameters used in models; $\alpha = \alpha_a + \alpha_s \approx af^b$. The scattering component for T1 is zero ($a_s = 0$), while for T2 it is half the attenuation ($\alpha_s = .5\alpha$).

Duck notes that scattering may account for 10%-15% of the observed attenuation in the low MHz range, and the proportion will increase with frequency. Scattering by fatty tissue is higher, in general [20].

Absorption is typically incorporated into time-domain simulations using classical viscous models, namely, stiffness- and mass-proportional damping, their linear combination called Rayleigh damping, and viscoelastic damping. Damping versus frequency for each is illustrated in Figure 2, where all are set equal at 5 MHz. These are linear models chosen for their operational and algorithmic properties rather than embodying or mimicking real absorption mechanisms in tissue, i.e., phenomenological. Energy absorbed in an element is found by accumulating the absorbed power increment over each timestep. The energy fraction converted to heat dose is given by α_a/α.

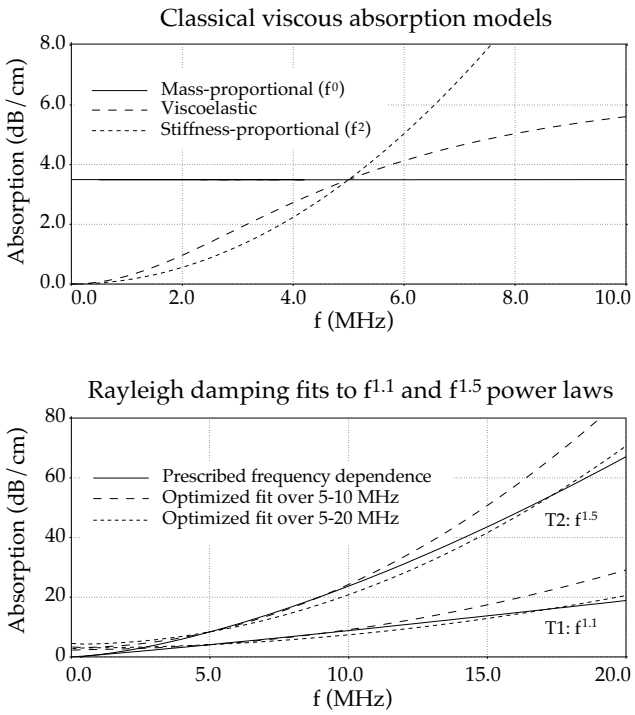

Figure 2. Absorption models used in time-domain wave propagation calculations (upper), and Rayleigh damping fits to frequency power laws (lower) for tissue parameters considered: T1 (muscle/tumor) and T2 (fatty tissue). All models match prescribed value at 5 MHz.

The difficulty with classical viscous damping models in the time-domain is that only exponents of 0 and 2 are represented exactly, by mass- and stiffness-proportional damping, respectively, while viscoelastic damping yields a range of exponents from 2 to 0 with increasing frequency. Multiple viscoelastic (relaxation) models can tailor the fit over a range of frequencies but this carries a high computational overhead. An adequate fit, in general, is given by Rayleigh damping, i.e., linear plus quadratic, because two constants are available. Fits to the tissue parameters in Table 1 are shown in the lower plot in Figure 2, where a is the value at 1 MHz. Water is fit "exactly" with stiffness-proportional damping.

Note that alternative damping models based on plasticity can also be postulated. For example, Kelly and Butler [21] conclude that their low frequency experimental data on intracellular damping is only compatible with viscoplasticity. However, since plastic behavior is nonlinear, this class of models has received little attention in focused ultrasound. Viscoplasticity shear-type models are available in the code and deserve future attention.

SHOCK PROPAGATION

As the spherically converging ultrasound beam propagates in lossy tissue, pressure is amplified by geometric focusing, modulated by diffraction, and attenuated by frequency-dependent absorption and scattering. Typical peak intensities for tissue ablation are from 1 to 3 kW/cm^2 at the focus, corresponding to focal pressures from 5.5 to 9.5 MPa. At these levels nonlinearity causes compression wave steepening and harmonic heating in the focal zone. Of interest here is the magnitude of these effects in typical applications.

Consider 1D propagation of a f = 4.75 MHz wave train in the Table 1 media. Initial pressure amplitude is A = 6.8 MPa (1000 psi), which is at the low end of focal levels used in laboratory and clinical equipment. Starting at time t = 0, pressure p = A sin(2πft) is applied to the end of a 1D, densely sampled (100 elements/wave length), long model. At least 15 elements per wavelength are necessary to propagate a wave with "negligible" numerical dispersion (wave speed dependence on wave length) for the piece wise-linear finite elements used here. Since this model has 100 elements per wave length of the fundamental, it should faithfully propagate the first 6 or 7 harmonics and rapidly disperse higher ones. Significant energy in higher harmonics will cause numerical oscillations (ringing) around the compression fronts. This is equivalent to under sampling of high gradients at the shocks.

Snapshots of the wave train in each medium are crossplotted in Figure 3 over windows from 3 to 5 mm and from 8 to 10 mm. Recall that negative pressure is compression. Harmonic generation by compressional wave steepening is obvious. In the 3-5 mm window water "shocks up" first, due to low absorption despite the lowest B/A, and the shock front is beginning to ring at around 4 mm, indicating harmonics above the 7th at this range. Ringing is removed from the water wave train over the 8-10 mm window by a smoothing algorithm that effectively damps spurious oscillations above the grid's numerical passband. We observe that the fatty tissue (T2) is also beginning to shock up at the 5 mm range, but its attenuation suppresses ringing.

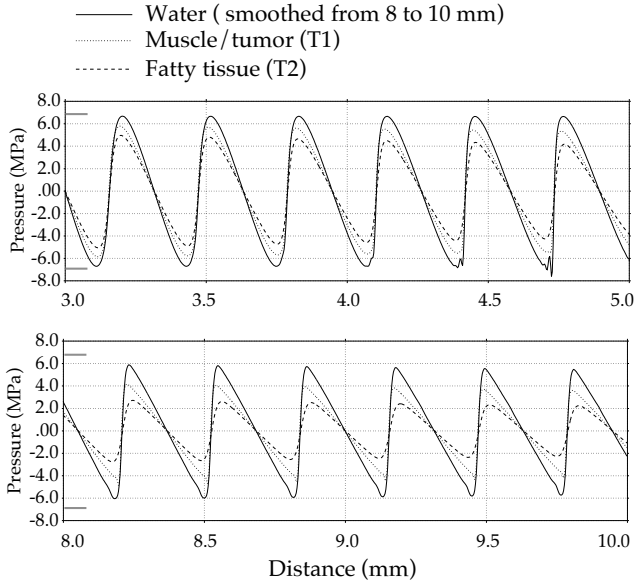

Figure 3. Snapshots of 4.75 MHz plane waves in nonlinear, 1D finite element models of water and tissue (see Table 1). Input pressure of 6.8 MPa (1000 psi) causes rapid steepening and harmonic generation. Ranges shown are 3-5 mm and 8-10 mm.

The smoothing algorithm applied to the water wave train is equivalent to artificial (quadratic) viscosity, and, indeed, shock phenomena calculated on discrete grids are usually stabilized using this approach [22]. We find our own conservative smoothing scheme [16] a better choice since it is uniformly effective in both fluids and solids without tuning. The amount of energy removed at the shock by smoothing is known but not easily converted to a thermal dose because the harmonic distribution is skewed by dispersion. In principle, analytical estimates can be made.

The harmonic distribution at a point in the model is given by the FFT of an integer number of pressure cycles there. Harmonic amplitudes at the 5 mm range for each of the cases in Figure 3 are shown in Figure 4. Significant harmonics above the 6th or 7th are not well resolved by this grid and cause ringing as noted above. It is possible to estimate the harmonic amplitudes analytically. For example, a heuristic analysis by Black in 1940 [23] yields the approximate plane wave relation

$$P_2 \approx \pi M P_1 \beta \frac{x}{\lambda} \quad ; \quad \beta \equiv 1 + \frac{B}{2A} \quad , \quad M \equiv \frac{v}{c_0} = \frac{P_1}{\rho_0 c_0^2} \quad (6)$$

between the first (P_1) and second (P_2) harmonic as a function of distance x in a nonattenuating media, where M is Mach number and v is particle velocity. More complete analyses are available but this will suffice for our purpose. We remark that the Mach number in water at 5 mm in Figure 3 is M=0.00267, the order of which confirms validity of the small-displacement algorithm in PZFlex for focused ultrasound simulations.

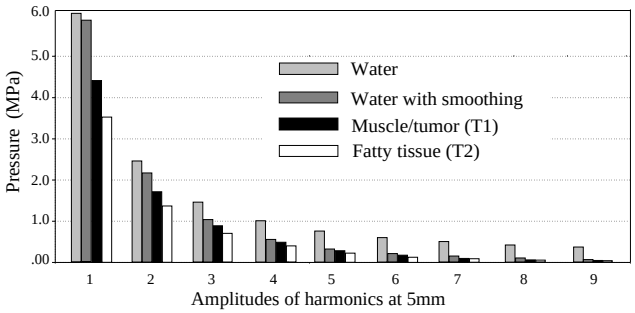

Figure 4. Harmonic amplitudes calculated at a range of 5 mm. Sizable harmonics above the 6th or 7th are not well resolved by the discrete grid (100 elements/fundamental wave length) and cause ringing. Second harmonics are consistent with theory.

Comparing P_2 from (6) to values in Figure 4, the calculated 2nd harmonics are lower by 10% in water and T1, and by 11% in the lossier T2. Considering Black's approximations this is a reasonable and consistent comparison. A conservative estimate of range $\tilde{x}$ for the onset of nonlinearity is found by setting $P_2 = \delta P_1$, $0 < \delta \le 0.5$, in (6), and solving as

$$\frac{\tilde{x}}{\lambda} = \frac{\delta}{\pi \beta M} \approx 0.716 \frac{10^9}{\beta P_1} \delta \quad (7)$$

Assuming an arbitrary 2nd harmonic threshold of δ = 0.3, say, then for 6.8 MPa, 4.75 MHz plane waves in water this indicates significant nonlinearity at 3 millimeters. At .68 kPa, corresponding to a power flux of 15.4 watts/cm^2, shocking would occur in 30 centimeters, and for 68 kPa or .154 watts/cm^2 it would take 3 meters. The presence of damping insures that these are conservative estimates. Considering that high pressure is limited to the focal region, as in Figure 1, such results suggest that propagation nonlinearity is negligible elsewhere.

THERMAL MODELING

Ultrasound power density on the order of kW/cm^2 in the focal region rapidly raises temperatures to ablation levels and can profoundly alter physical properties. Analysis of this transient process involves the following steps:

1) calculate initial, steady ultrasound field and thermal dose per time step (or cycle or unit time);
2) solve for the transient temperature field and apply to lesion evolution and/or thermal-mechanical constitutive models;
3) if indicated, apply incremental temperature effects to thermal and mechanical tissue properties and repeat steps 1-3.

If mechanical properties are not affected by the temperature levels then ultrasound and thermal fields are decoupled and the calculation stops at step 2). Most analyses assume so and take thermal dose q (heat source function) proportional to a given, unchanging, albeit attenuated, intensity field as $q = 2\alpha I = \alpha p^2/\rho c$ (α in nepers/m = dB/cm/MHz^2/0.08686). This is fine for low absorption and moderate temperatures [24], but under more extreme conditions it is necessary to take step 3) and solve the coupled problems incrementally.

For an example of steps 1 and 2 in the modeling process consider the ocular tumor application reported by Lizzi, et al. [25]. The axisymmetric model, illustrated in Figure 5, is a malignant melanoma (T1, Table 1) in the rear segment of the eye, with vitreous humor in front (water, Table 1) and backed by orbital fat (T2, Table 1). A snapshot of the 4.75 MHz ultrasound field propagating through the vitreous humor and focused in the tumor is superposed on the top half. Peak intensity is 1.05 kW/cm^2. The temperature distribution after 3 sec of exposure is superposed on the bottom half. Observe that this yields temperatures above 100°C at the focus.

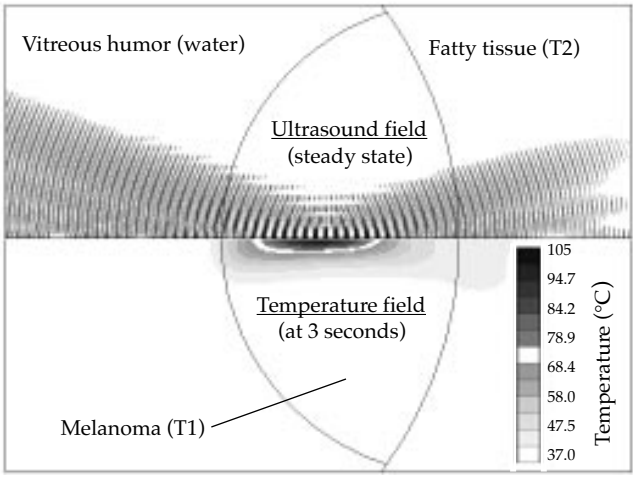

Figure 5. Axisymmetric model of an ocular tumor, showing focused ultrasound beam (above) and temperature distribution at 3 sec (below). Note focal temperature in excess of 100 °C. The transducer has a 4 cm aperture and 9 cm focal length.

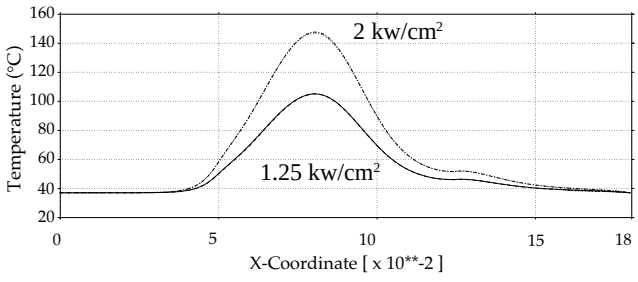

Figure 6. Temperature calculated on the axis through the focal zone in Fig. 5 with and without propagation nonlinearity (B/A). Intensities are 1.25 and 2.0 kW/cm^2 in melanoma (T1). Harmonic heating in this tissue is seen to be negligible.

The focused ultrasound field in Figure 5 is from a spherical transducer with 4 cm aperture and 9 cm radius (f/2.25). Time harmonic pressure from a theoretical diffraction calculation is applied to the left boundary of this focal zone model, starting at t = 0 and continuing to steady-state (t ≈ 27 μsec, Δt ≈ 13 nsec). Observe the rapid attenuation in fatty tissue to the right.

A series of linear and nonlinear (B/A) calculations were done in this model to quantify effects on axial temperature peaks. These are shown in Figure 6 for melanoma at 1.25 and 2.0 kW/cm^2 peak Temperature enhancement by harmonic heating at 2.0 kW/cm^2 is insignificant because the 2nd harmonic is only 18% of the first and the 3rd is negligible.In general, since the focal zone is only a few wave lengths deep, thre is little opportunity for significant harmonic generation, even at 4-6 kW/cm^2.

BUBBLE MODEL

For an example of step 3 in the thermal modeling process we consider the impact of temperatures above boiling in the focal zone of the model in Figure 5. This affects absorption through elevated temperature or coagulation, and cavitation-induced sound speed changes. Given the paucity of data we consider a hypothetical cavitation or "boiling" mechanism for reduced sound speed. Assume that at some temperature T_b at or above boiling, microbubbles form by cavitation or superheating within the focal tissue's T_b isotherm. Assume further that the volume fraction of bubbles is small but sufficient to reduce bulk modulus substantially, say by factors of 10 or more, while tissue density decreases only slightly. Therefore, the speed of sound, $\sqrt{k/\rho}$, and acoustic impedance will be reduced by at least a factor of 3. This effect, analyzed in [26] for bubbles in a fluid, makes the tissue dispersive and depends on bubble size and number, and ultrasound frequency. It is readily measured and the theory has been confirmed by experiments [27].

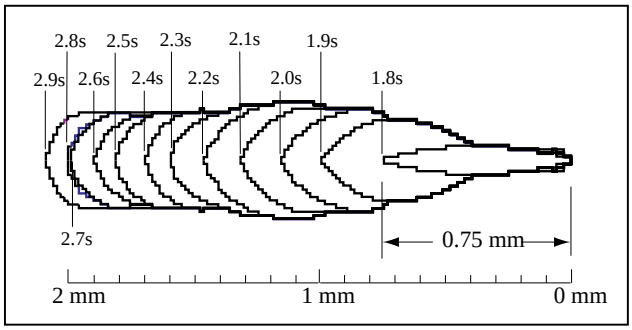

Figure 7. Calculated spread of a superheated, bubbly region from the focus, using 0.1 sec time increments. The region evolves on an element-by-element basis from within the T_b = 100°C isotherm by zeroing stiffness when $T > T_b$.

To model a first order example of this mechanism we calculate the temperature increase driven by the steady ultrasound field in Figure 5. When one or more elements reach T_b = 100°C they are cavitated, i.e., stiffness is reduced, and the ultrasound propagation calculation is repeated. A new dose is determined from the modified steady state ultrasound field, temperature is recalculated, a modified distribution of elements eventually reach T_b, and the calculations are repeated. Since there is a great disparity in sound and thermal time scales, it is unnecessary to run the two calculations together.

Instead, the ultrasound model is rerun to steady-state after each significant increment of thermal-induced change.

Results of such a calculation are shown in Figure 7 for the low dose case in Figure 5. Sound speed in a cavitated element is assumed to be zero rather than finite, e.g., the factor of 3 mentioned above—for the sake of simplicity since experiments show an impedance contrast high enough to reflect most of the ultrasound [7,8]. The time increment between ultrasound recalculations is set to 0.1 sec—for simplicity again. The figure shows the bubbly region filling out the focal zone contour until 1.8 sec. Between 1.8 and 1.9 sec it abruptly inflates into the pre-focus and subsequently expands almost uniformly towards the transducer. It begins to slow at 2.5 sec, stalls at 2.7 sec, and expands again. A smaller time increment is no doubt appropriate, particularly during the rapid inflation from 1.8 to 1.9 sec and the stall at 2.7 to 2.8 sec.

DISCUSSION

The numerical experiments described above demonstrate the utility of a general purpose, time-domain finite element code for incrementally linear solutions of fundamentally nonlinear phenomena in focused ultrasound tissue ablation.

We have shown that full models of a complicated piezoelectric transducer, travel path, and focal zone are practical. When a full simulation is impractical for reasons of limited memory or computer time, models can be localized around essential regions or structures with their fields "connected" analytically or numerically. More to the point, nonlinear propagation phenomena are well solved by the incrementally linear method, as are more severe nonlinear phenomena, exemplified by the calculation of a bubbly region expanding into the prefocal zone.

In addition to demonstrating capability, our results provide partial answers to some nagging questions. In particular, for f-numbers and intensities typical of transducers in use today, shocking/harmonic generation along the travel path does not appear significant; nor does harmonic heating at the focus, except at very high intensities. The question of a gas body as the limiting factor in tissue ablation has been addressed, at least suggestively. With a heuristic mechanism identified, a working model, and experimental data we can begin to explore related boiling/cavitation phenomena. For example, rapid inflation of a bubbly region by cavitation should produce sound. Crum and Law [28] have observed this type of acoustic emission and we should be able to use it to infer temporal and spatial details of the actual process and refine our model.

ACKNOWLEDGMENT

This work was supported in part under NIH SBIR Grant 1R43CA65255 and NSF SBIR Grant DMI-9313666 (G.W., J.M., N.A., D.V.) and NIH Research Grant IR01Y10369 (F.L, M.O.).

REFERENCES

[1] W.J. Fry, W.H. Mosberg, J.W. Barnard, and F.J. Fry, "Production of focal destructive lesions in the central nervous system with ultrasound," *J. Neurosurg.*, **11**, 471-478, 1954.

[2] R. Heimburger, "Ultrasound augmentation of central nervous system tumor therapy," *Indiana Med.*, 469-476, June 1985.

[3] N.T. Sanghvi, F.J. Fry, J.F. Huddleston, R.F. Morris, and S.A. Goss, "Ultrasound system for noninvasive focal lesioning in organs and tissue," *J. Ultrasound Med.*, **3**, S30, 1984.

[4] E. Purnell, A. Sokollu, R. Torchia, and N. Taner, "Focal chorioretinitis produced by ultrasound," *Invest. Ophthalmol.*, **3**, 657-664, 1964.

[5] F.L. Lizzi, D.J. Coleman, J. Driller, M. Ostromogilsky, S. Chang, and P. Greenall, "Ultrasonic hyperthermia for ophthalmic therapy,", *IEEE Trans. Sonics Ultrasonics*, **31**, 473-481, 1984.

[6] R.S. Foster, R. Bihrle, N.T. Sanghvi, F.J. Fry, S.L. Griffith, A.M. Snoddy, and T.D. Franklin, "Noninvasive ultrasound produced volume lesion in prostate," *Symp. ESWL*, Washington, 1990.

[7] F.J. Fry, "Intense focused ultrasound in medicine," *Eur. Urol.*, **23**, 2-7, 1993.

[8] F.L. Lizzi, D.J. Coleman, J. Driller, R.H. Silverman, B. Lucas, and A. Rosado, " A therapeutic ultrasound system incorporating real-time ultrasonic scanning," in Proc. of the 1986 Ultrasonics Symposium, B.R. McAvoy (ed.), IEEE, New York, 1987.

[9] F.L. Lizzi, "High-precision thermotherapy for small lesions," *Eur. Urol.*, **23** (suppl. 1), 23-28, 1993.

[10] E. Vallencien, Chartier-Kastler, N. Bataille, D. Chopin, M. Harouni, and J. Bougaran, "Focused extracorporeal pyrotherapy," *Eur. Urol.*, **23** (suppl. 1), 48-52, 1993.

[11] C.A. Damianou, K. Hynynen, and X. Fan, "Evaluation of accuracy of a theoretical model for predicting the necrosed tissue volume during focused ultrasound surgery," *IEEE Trans. Ultrason., Ferroelect. and Freq. Control*, **42**, 182-187, 1995.

[12] P.T. Christopher and K.J. Parker, "New approaches to nonlinear diffractive field propagation," *J. acoust. Soc. Am.*, **90**, 488-499, 1991.

[13] S.I. Aanonsen, "Numerical computation of the nearfield of a finite amplitude sound beam," Rep. #73, Dept. of Mathematics, University of Bergen, 1983.

[14] G.L. Wojcik, D.K. Vaughan, N. Abboud, and J. Mould, Jr., "Electromechanical modeling using explicit time-domain finite elements," *Proc. IEEE Ultrasonic Symp.*, **2**, 1107-1112, 1993.

[15] C.I. Zanelli, C.W. Hennige, and N.T. Sanghvi, "Design and characterization of a 10 cm annular array transducer for high intensity focused ultrasound (HIFU) applications," *Proc. IEEE Ultrasonic Symp.*, **3**, 1887-1890, 1994.

[16] I.S. Sandler and D. Rubin, "FUSE calculations of far-field water shock including surface and bottom effects," Weidlinger Associates Tech. Report to SAIC/Pacifica Technology Div., San Diego, CA, 1990.

[17] R.T. Beyer, Nonlinear Acoustics, Naval Sea Systems Command, 1974. Government Printing Office, Washing-ton, D.C., #0-596-215, 1975.

[18] H.H. Pennes, "Analysis of tissue and arterial blood temperatures in the resting human forearm," *J. Appl. Physiol.*, **1**, 93-122, 1948.

[19] F.A. Duck, Physical Properties of Tissue, Academic Press, 1990.

[20] F.T. D'Astous and F.S. Foster, "Frequency dependence of ultrasound attenuation and backscatter in breast tissue," *Ultrasound Med. Biol.*, **12**, 795, 1986.

[21] S. Kelly and J. Butler, *Private Communication*, Harvard School of Public Health, Physiology Program, 1995.

[22] J. Von Neumann and R.D. Richtmeyer, " A method for the numerical calculation of hydrodynamic shocks," *J. Appl. Phys.*, **21**, 1950.

[23] L.J. Black, "Physical analysis of distortion produced by the nonlinearity of the medium," *J. Acoust. Soc. Am.* **34**, 1254-1264, 1940.

[24] W.L. Nyborg, "Heat generation by ultrasound in a relaxing medium," *J. Acoust. Soc. Am.*, **70**, 330, 1981.

[25] F.L. Lizzi, J. Driller, B. Lunzer, A. Kalisz, and D.J. Coleman, "Computer model of ultrasonic hyperthermia and ablation for ocular tumors using B-mode data," *Ultrasound in Med. & Biol.* **18**, 59-73, 1992.

[26] T.G. Leighton, The Acoustic Bubble, Academic Press, 1994.

[27] S.A. Cheyne, C.T. Steffijs, and R.A. Roy, "Phase velocity measurements in bubbly liquids using a fiber opticlaser interferometer," J. Acoust. Soc. Am., 97, 1621-1624, 1995.

[28] L. Crum and W. Law, *Private Communication*, Focus Surgery, Milpitas, CA, 1995.